

1 **Tropospheric warming over the North Indian Ocean caused by the South Asian**
2 **anthropogenic aerosols: possible impact on the upper troposphere and lower**
3 **stratosphere**

4
5 Suvarna Fadnavis^{1*}, Prashant Chavan¹, Akash Joshi², Sunil Sonbawne¹, Asutosh Acharya³,
6 Panuganti C S. Devara⁴, Alexandru Rap⁵, Felix Ploeger⁶ and Rolf Müller⁶

7 ¹Indian Institute of Tropical meteorology, MoES, Pune, India

8 ²Indian Institute of Technology, Kharagpur, India

9 ³Indian Institute of Technology, Bhubneshwar, India

10 ⁴Centre of Excellence in ACOAST/ACESH, Amity University Haryana (AUH), Gurugram
11 122413, India

12 ⁵School of Earth and Environment, University of Leeds, Leeds, United Kingdom

13 ⁶Forschungszentrum Jülich GmbH, IEK-7, Jülich, Germany

14 Corresponding author: Suvarna Fadnavis

15 Corresponding author email: suvarna@tropmet.res.in

16
17
18 **Abstract**

19 Atmospheric concentrations of South Asian anthropogenic aerosols and their transport play a
20 key role in the regional hydrological cycle. Here, we use the ECHAM6-HAMMOZ
21 chemistry-climate model to show the structure and implications of the transport pathways of
22 these aerosols during spring (March-May). Our simulations indicate that large amounts of
23 anthropogenic aerosols are transported from South Asia to the North Indian Ocean and
24 Western Pacific. These aerosols are then lifted into the upper troposphere and lower
25 stratosphere (UTLS) by the ascending branch of the Hadley circulation, where they enter the
26 westerly jet. They are further transported to the Southern Hemisphere (~15° S – 30° S), and
27 downward (320 – 340K) via westerly ducts over the tropical Atlantic (5° S – 5° N, 10° W – 40°
28 W) and Pacific (5° S – 5° N, 95° E – 140° E). The carbonaceous aerosols are also transported to
29 the Arctic leading to local heating (0.08 – 0.3 K month⁻¹, an increase by 10 – 60 %).

30 The presence of anthropogenic aerosols causes a negative radiative forcing (RF) at the TOA
31 ($-0.90 \pm 0.089 \text{ W m}^{-2}$) and surface ($-5.87 \pm 0.31 \text{ W m}^{-2}$) and atmospheric warming ($+4.96 \pm 0.24$
32 W m^{-2}) over South Asia ($60^\circ \text{ E} - 90^\circ \text{ E}$, $8^\circ \text{ N} - 23^\circ \text{ N}$), except over the Indo-Gangetic plain
33 ($75^\circ \text{ E} - 83^\circ \text{ E}$, $23^\circ \text{ N} - 30^\circ \text{ N}$) where RF at the TOA is positive ($+1.27 \pm 0.16 \text{ W m}^{-2}$) due to
34 large concentrations of absorbing aerosols. The carbonaceous aerosols lead to in-atmospheric
35 heating along the aerosol column extending from the boundary layer to the upper troposphere
36 (0.1 to 0.4 K month^{-1} , increase by 4 – 60 %) and in the lower stratosphere $40^\circ \text{ S} - 90^\circ \text{ N}$ (0.02
37 to 0.3 K month^{-1} , increase by 10 – 60 %). The increase in tropospheric heating due to aerosols
38 results in an increase in water vapor concentrations, which are then transported from the
39 North Indian Ocean-Western Pacific to the UTLS over $45^\circ \text{ S} - 45^\circ \text{ N}$ (increasing water vapor
40 by 1 - 10 %).

41 Keywords: South Asian Anthropogenic aerosols; warming over the Arabian Sea; transport of
42 aerosols and water vapor to the UTLS in spring.

43 **1. Introduction**

44 Understanding the variability of anthropogenic aerosol loading over the North Indian
45 Ocean is of utmost importance since (1) it regulates the Asian hydrological cycle via
46 modulating atmospheric convection, heating rates, and moisture transport (Ramanathan et al.,
47 2005; Corrigan et al., 2008; Budhavant et al., 2018, Meehl et al., 2008), and (2) it leads to
48 adverse impacts on marine ecosystems (Mahowald et al., 2018; Collins et al., 2019). Several
49 observations indicate that the aerosol loading over the North Indian Ocean during the spring
50 season is strongly influenced by South Asian aerosols. Aircraft measurements during the
51 Indian Ocean Experiment (INDOEX) (February–March 1999) showed the presence of a thick
52 layer (surface to 3.2 km) of anthropogenic aerosols (BC~14 %, sulfate 34 %, ammonium 11
53 %) over the North Indian Ocean (Dickerson et al., 2002; Mayol-Bracero et al., 2002) with
54 sources over South Asia. Several other in situ observations, e.g. over the Maldives during
55 November 2014 – March 2015, show that air masses arising from the Indo-Gangetic Plain
56 contain very high amounts (97 %) of the elemental carbon in the PM₁₀ in the fine mode.
57 (Bhuhvant et al., 2018). Observations from the Geosphere-Biosphere Programme over the
58 Bay of Bengal during spring (March 2016) also show abundant anthropogenic aerosols
59 (sulfate and nitrate) having sources over the Indo-Gangetic plain (Nair et al., 2017).

60 The aerosol loading over South Asia has been increasing at an alarming rate (rate of
61 increase in AOD 0.004 per year during 1988 – 2013) (Babu et al., 2013). For the last two
62 decades, the AOD increase (by 12 %) over South Asia has been attributed to the strong
63 increase in anthropogenic aerosols (sulfate, black carbon, and organic carbon), while natural
64 aerosol remained unchanged (Ramachandran et al., 2020a). The major sources of
65 anthropogenic aerosols are the combustion of domestic fuels, industrial emissions,
66 transportation, and open burning (Paliwal et al., 2016). The growth of the economy of India

67 led to a 41 % increase in BC and 35 % in OC from 2000 to 2010 (Lu et al., 2011). The
68 emissions of sulfur dioxide (SO₂) which leads to the production of sulfate aerosols have
69 doubled during 2006 – 2017 (Fadnavis et al., 2019). Figure 1 a-c shows the annual mean
70 emission of BC, OC, and sulfate aerosols over South Asia in 2016 from AEROCOM-
71 ACCMIP-II emission inventory (discussed in section 2.1). It shows high emissions over the
72 Indo-Gangetic Plain (BC 7×10^{-12} – 17×10^{-12} Kg m⁻² S⁻¹, OC: 25×10^{-12} - 70×10^{-12} Kg m⁻² S⁻¹,
73 sulfate: 2×10^{-12} - 5×10^{-12} Kg m⁻² S⁻¹). Higher amounts of aerosols over the Indo-Gangetic
74 Plain are associated with densely populated regions and industrial and vehicular emissions
75 (Karambelas et al., 2018, Fadnavis et al., 2019). Past studies also show substantially higher
76 amounts of aerosols over North India compared to the rest of the Indian region
77 (Ramachandran et al., 2020b, Fadnavis et al., 2013, 2017a, 2017b). Over the Indo-Gangetic
78 plain, these emissions show a peak in spring (Fig. 1d), with increases for BC of 0 – 3 %, OC
79 0 – 8.7 %, and sulfate 0 – 0.2 %, compared to annual means. This peak in emissions in spring
80 is to a large extent driven by springtime agricultural crop burning and biomass burning
81 activity (Chavan et al., 2021).

82 While the presence of sulfate aerosols leads to a cooling of the atmosphere below due to
83 their strong scattering properties, carbonaceous aerosols produce atmospheric warming via
84 absorption of solar radiation (Fadnavis et al., 2019, Penner et al., 1998). Previous studies
85 showed that the doubling of carbonaceous aerosols loading over South Asia (10° S – 50° N,
86 65° E – 155° E) led to significant atmospheric warming (in-atmospheric RF 5.11W m⁻²,
87 Fadnavis et al. 2017b).

88

89

90

91

92

93

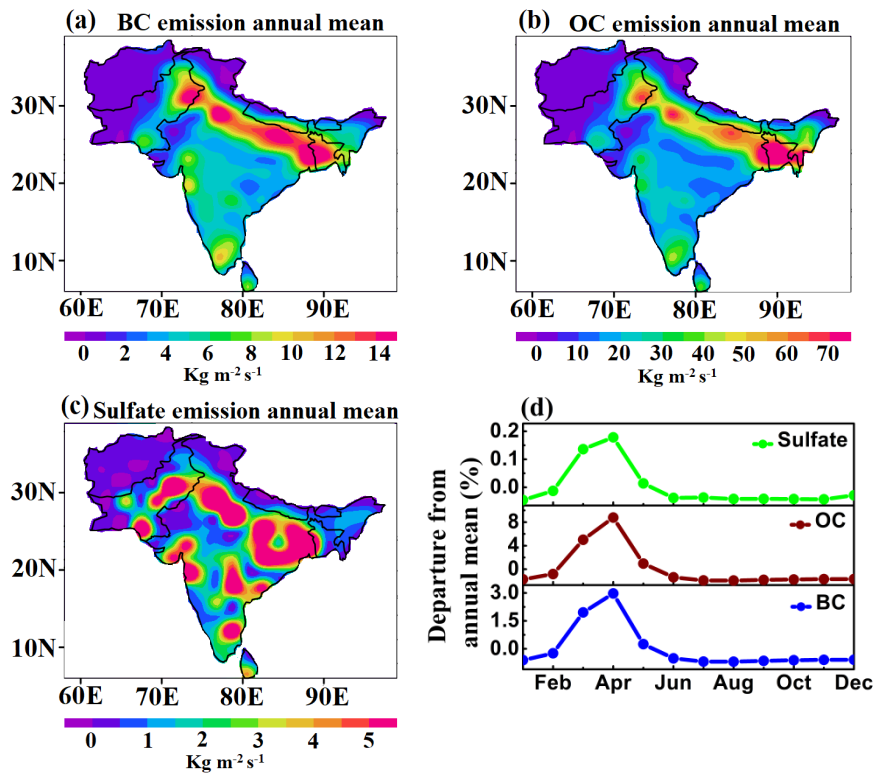
94

95

96

97

98



99 Figure 1: Spatial distribution for the year 2016 annual mean total emission ($\text{kg m}^{-2} \text{S}^{-1}$) of
100 (a) BC, (b) OC, (c) Sulfate aerosols from AEROCOM-ACCMIP-II emission inventory, (d)
101 time series of monthly departure from annual mean total emissions (%) of BC, OC, and
102 Sulfate aerosols averaged over Indo-Gangetic plain ($23^\circ \text{N} - 30^\circ \text{N}$, $78^\circ \text{E} - 90^\circ \text{E}$).

103

104 During spring, the prevailing convective instability over the Bay of Bengal and the
105 Arabian Sea transports aerosol from the boundary layer to the upper troposphere
106 (Romatschke and Houze, 2011). Airborne observations during winter and spring, e.g. the
107 Civil Aircraft for Regular Investigation of the Atmosphere based on an Instrument Container
108 (CARIBIC) in March 1999 and January 2001 (Papasiropoulos et al., 2002), and the Indian
109 Ocean Experiment (INDOEX) in February-March 1999 show elevated aerosol amounts near
110 8 – 12 km over the Indian Ocean and South Asia (De Reus et al., 2001). Recently, using a set
111 of model simulations, Chavan et al., (2021) reported the transport of biomass burning
112 aerosols to the upper troposphere by convection in spring 2013.

113 Here, we investigate the source of the very large aerosol loading over the Arabian Sea
114 during spring and, their vertical transport to the UTLS. We show these aerosols produce
115 atmospheric warming leading to enhanced water vapor that is transported to the UTLS. Once
116 in the lower stratosphere, aerosols and water vapour are transported to the Southern
117 hemisphere ($\sim 45^\circ$ S), with implications on tropospheric temperatures and stratospheric ozone
118 concentrations. For this purpose, we performed a series of five simulations using the
119 ECHAM6-HAMMOZ model in order to investigate the impact of changes in anthropogenic
120 aerosol over South Asia. The paper is structured as follows: the ECHAM6-HAMMOZ model
121 simulations are provided in section 2, in section 3 we discuss the results on the transport of
122 South Asian aerosols to the North Indian Ocean, radiative forcing, transport into the UTLS,
123 and associated impacts on heating rates, while conclusions are summarised in section 4.

124 **2. Model simulations**

125 **2.1 ECHAM6-HAMMOZ experimental set-up**

126 We use the state of the art aerosol–chemistry–climate model ECHAM6–HAMMOZ. It
127 comprises of the general circulation module ECHAM6, coupled to the aerosol and cloud
128 microphysics module Hamburg (HAM) (Stier et al., 2005; Tegen et al., 2019). HAM
129 predicts the nucleation, growth, evolution, and sinks of sulfate, black carbon (BC), organic
130 carbon (OC), sea salt (SS), and mineral dust (DU) aerosols. The size distribution of the
131 aerosol population is described by seven log-normal modes (Nucleation mode, soluble and
132 insoluble Aitken, soluble and insoluble accumulation and soluble and insoluble coarse
133 modes) (Stier et al., 2005; Zhang et al., 2012; Tegen et al., 2019). Moreover, HAM
134 explicitly simulates the impact of aerosol species on cloud droplet and ice crystal formation
135 according to prescribed microphysical properties. Aerosol particles can act as cloud
136 condensation nuclei or as kernel for ice-nucleating particles. Other relevant cloud

137 microphysical processes such as evaporation of cloud droplets, sublimation of ice crystals,
138 ice crystal sedimentation, and detrainment of ice crystals from convective cloud tops are
139 simulated interactively (Neubauer et al., 2014). The anthropogenic and fire emissions of
140 sulfate, black carbon (BC), and organic carbon (OC) are based on the AEROCOM-
141 ACCMIP-II emission inventory. Other details of the model and emissions are reported by
142 Fadnavis et al. (2017a, 2019, 2021a, b).

143 The model simulations are performed at a T63 spectral resolution corresponding to
144 $1.875^\circ \times 1.875^\circ$ in the horizontal dimension, while the vertical resolution is described by 47
145 hybrid σ -p levels from the surface up to 0.01 hPa (approx. 80 km). The simulations have
146 been carried out with a time step of 20 min. Monthly varying Atmospheric Model Inter-
147 comparison Project (AMIP) sea surface temperature (SST) and sea ice cover (SIC) (Taylor et
148 al., 2000) were used as lower boundary conditions.

149 We performed five model experiments: (1) a control (CTL) simulation where all aerosol
150 emissions are included and four perturbed experiments where (2) all anthropogenic aerosol
151 emissions (black carbon, organic carbon, and sulfate) are switched off over South Asia (75° E
152 $- 100^\circ$ E, 8° N $- 40^\circ$ N, see Fig. 1) during the study period (2001 $-$ 2016) (referred to as
153 Aerooff), (3) only anthropogenic black carbon emissions (BC) switched off during the study
154 period, (BCoff), (4) only anthropogenic organic carbon (OC) emissions switched off (OCoff)
155 during the study period, and (5) only anthropogenic sulfate aerosol emissions switched off
156 (Suloff) during the study period (see Table 1). All simulations were performed from 1
157 January 2001 to December 2016 from stabilized initial fields created after a model integration
158 for one year. Dust emission parameterization is the same in all the simulations and is based
159 on Tegen et al. (2002). The analysis is performed for spring (March $-$ May) averaged for the
160 period 2001 $-$ 2016. We compare the CTL with Aerooff, BCoff, OCOff, and Suloff
161 simulations to understand (1) transport path ways of South Asian anthropogenic aerosols, and

162 (2) their impact over the Indian region, and UTLS (340K – 400K). We compare AOD from
 163 CTL simulations with MISR and MODIS data (section S1). The model performance against
 164 MISR and MODIS (Kahn et al., 2007) for the spring season is discussed in section S2 from
 165 Fig. S1. We use the 2 PV contour in mid-latitudes and the 380 K isentrope in the tropics as an
 166 estimate of the location of the dynamical tropopause (Holton et al., 1995). Note that the PV
 167 value at the dynamical tropopause is often somewhat higher than 2 PV and exhibits a certain
 168 variability (Kunz et al., 2011).

169 Table -1: Details of ECHAM6-HAMMOZ model simulations performed in this study.

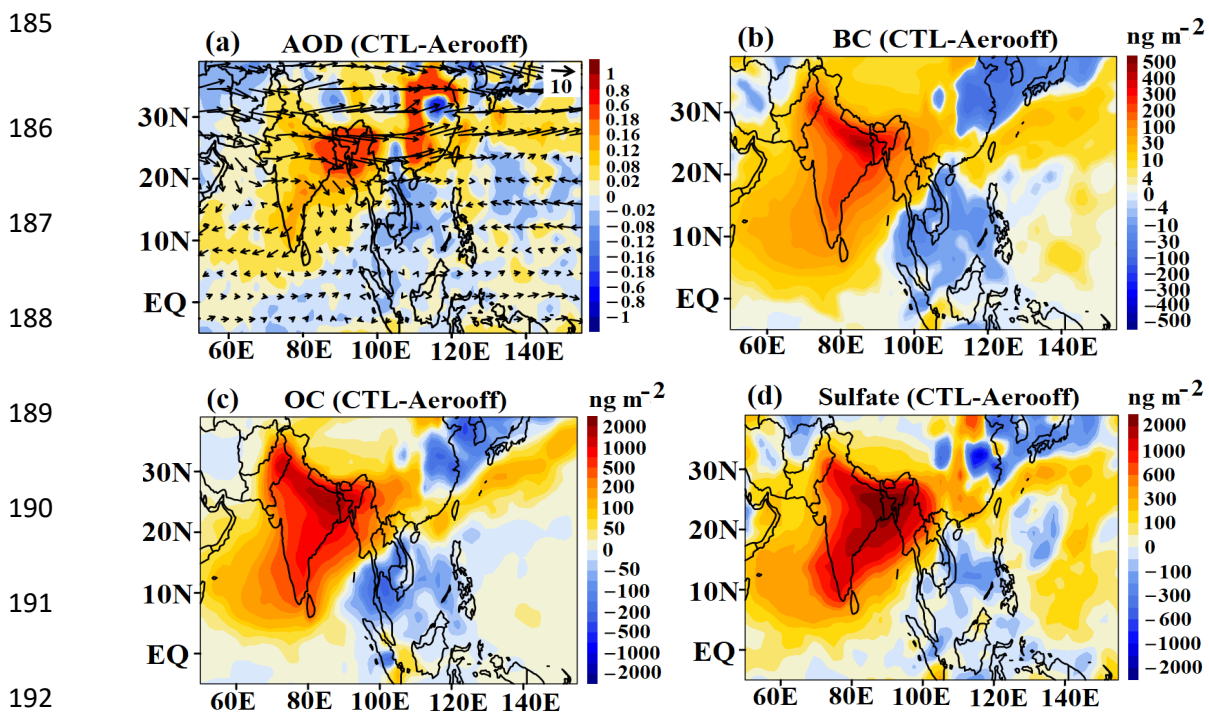
Experiment name	Duration	Aerosol species on/off	Boundary conditions
CTL	2001 – 2016	All aerosols species globally, as per AEROCOM-ACCMIP-II emission inventory.	AMIP Sea surface temperature and sea ice concentration.
Aerooff	2001 – 2016	Anthropogenic BC, OC, and sulfate aerosols switch off over South Asia during 2001 – 2016.	AMIP Sea surface temperature and sea ice concentration.
BCoff	2001 – 2016	Anthropogenic BC aerosols switch off over South Asia during 2001 – 2016.	AMIP Sea surface temperature and sea ice concentration.
OCoff	2001 – 2016	Anthropogenic OC aerosols switch off over South Asia during 2001 – 2016.	AMIP Sea surface temperature and sea ice concentration.
Suloff	2001 – 2016	Anthropogenic sulfate aerosols switch off over South Asia during 2001 – 2016.	AMIP Sea surface temperature and sea ice concentration.

170 3. Results and discussions

171 3.1 Transport of South Asian aerosols to the North Indian Ocean

172 The spatial distribution of AOD anomalies from the CTL-Aerooff simulation shows
 173 positive anomalies of AOD extending from South Asia to the Arabian Sea and the North Bay

174 of Bengal (10° N - 20° N) (Fig. 2a). The wind vectors indicate that these are transported from
 175 the Indo-Gangetic plain to the Arabian Sea, the Bay of Bengal and Western Pacific. The
 176 transported aerosols enhanced the AOD by 0.18 - 0.8 (30 - 80 %) over the North Bay of
 177 Bengal and by 0.02 - 0.12 (20 - 60 %) over the Arabian Sea. This is consistent with previous
 178 studies where 50 - 60 % enhancements in the AOD over the tropical Indian Ocean due to
 179 anthropogenic aerosols have been reported (Satheesh et al. 2000; Jose et al. 2020). Chemical
 180 analysis of aerosols observed over the south-eastern coastal Arabian Sea also shows the
 181 dominance of anthropogenic aerosols having sources over the Indian region (73 %) (Aswini
 182 et al., 2020). Analysis of MODIS satellite observations (2003 - 2017) likewise shows that
 183 anthropogenic sources contributed $\sim 60 - 70\%$ to the aerosol loading over the east coast and
 184 west coast of India (Jose et al. 2020).



193 Figure 2: Spatial distribution of (a) AOD anomalies averaged for spring during 2001 -
 194 2016 (CTL - Aerooff), and anomalies of tropospheric column of (b) BC, (c) OC, and (d)
 195 sulfate aerosols (ng m^{-2}) (CTL-Aerooff). The vectors in Fig.2a indicate winds (m s^{-1}) at
 196 850 hPa.

197

198 The distribution of anomalies of the tropospheric column of BC, OC, and sulfate aerosols
199 also indicates that these aerosols are transported from South Asia to the Bay of Bengal and
200 the Arabian Sea (Fig. 2b-d). Enhancement of sulfate and OC aerosol ($50 - 2000 \text{ ng m}^{-2}$) is
201 higher than BC ($4 - 500 \text{ ng m}^{-2}$) over the South Asian region (Fig. 2b-d). The total
202 carbonaceous aerosol (BC and OC together) dominates over the sulfate aerosols. These
203 anthropogenic aerosols over the tropical Indian Ocean affect the radiation budget and cloud
204 cover over the Indian Ocean (Satheesh et al., 2000; McFarquhar and Wang, 2006).

205 **3.2. Radiative forcing**

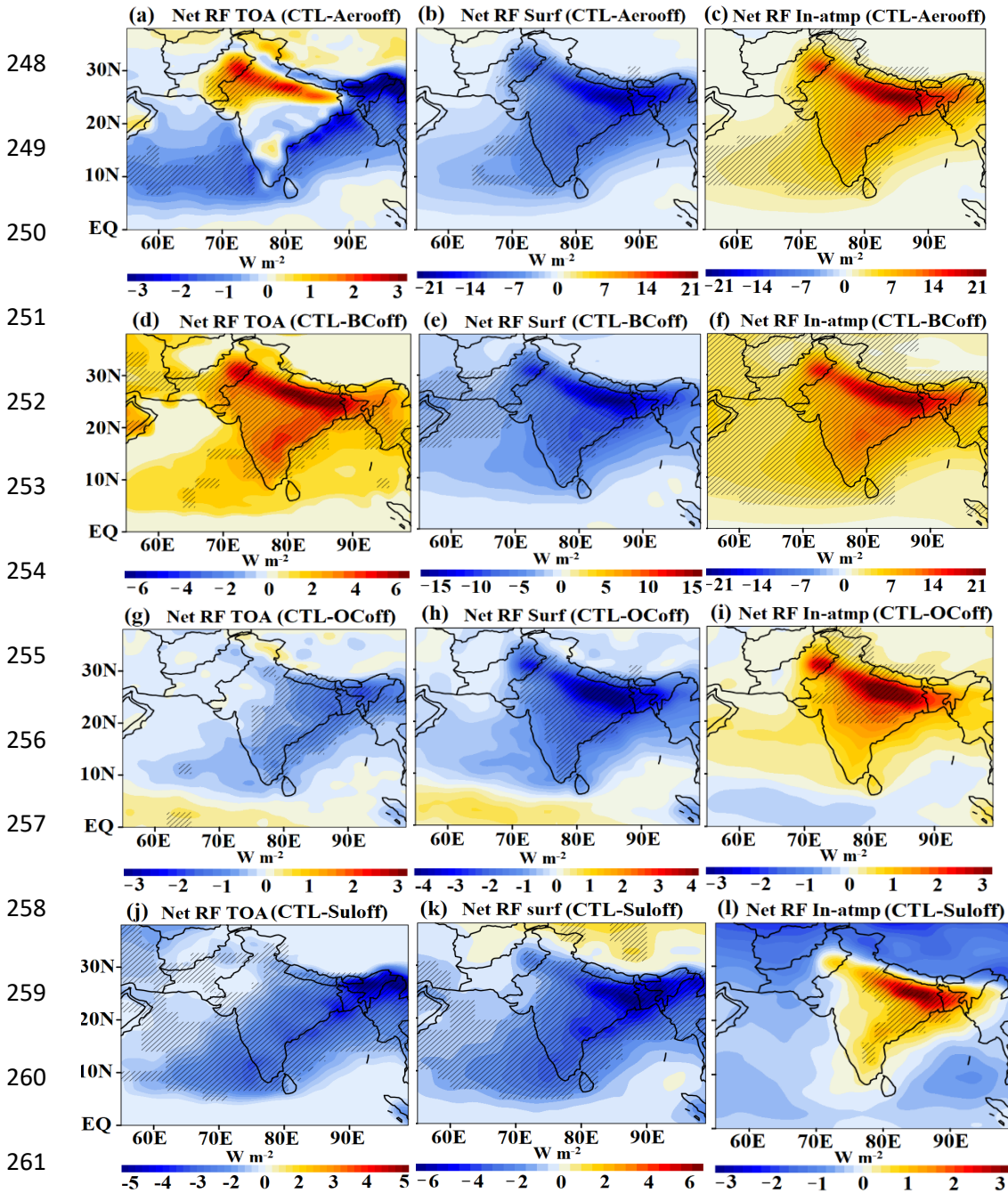
206 The anthropogenic aerosols over the tropical Indian Ocean affect the radiation budget and
207 cloud cover (McFarquhar and Wang, 2006). Here, we discuss the impact of South Asian
208 anthropogenic aerosols on RF. Figures 3a-c show anomalies in net RF at the TOA, surface,
209 and in-atmosphere (TOA - surface) for Aerooff simulations (CTL - Aerooff). The
210 anthropogenic aerosols have produced a cooling at the TOA (except over the Indo-Gangetic
211 plain) and at the surface (see Fig. 3a-b). The simulated RF values over the Arabian Sea (55°
212 $E - 70^\circ E$, $8^\circ N - 20^\circ N$), Bay of Bengal ($88^\circ E - 92^\circ E$, $12^\circ N - 20^\circ N$), and Indo-Gangetic
213 Plain ($75^\circ E - 83^\circ E$, $26^\circ N - 30^\circ N$) are tabulated in Table-S1. The RF estimates show that
214 the aerosols have produced cooling at the TOA and surface over the Arabian Sea (TOA: -
215 $0.72 \pm 0.14 \text{ W m}^{-2}$, surface: $-3.0 \pm 0.28 \text{ W m}^{-2}$), Bay of Bengal (TOA: $-1.24 \pm 0.15 \text{ W m}^{-2}$, surface:
216 $-5.14 \pm 0.44 \text{ W m}^{-2}$), and in-atmospheric warming over the above regions (Arabian Sea
217 $+2.27 \pm 0.19 \text{ W m}^{-2}$; Bay of Bengal: $+3.89 \pm 0.30 \text{ W m}^{-2}$) (Fig. 3 c). The Indo Gangetic Plain
218 shows positive anomalies of RF at the TOA ($+1.27 \pm 0.16 \text{ W m}^{-2}$), negative at the surface (-
219 $11.16 \pm 0.50 \text{ W m}^{-2}$), and an atmospheric warming of $+12.44 \pm 0.42 \text{ W m}^{-2}$. In agreement with
220 our results, previous studies have reported negative RF at the surface and TOA, and
221 atmospheric warming over the North Indian Ocean caused by enhanced anthropogenic
222 aerosol. For example, Pathak et al. (2020) reported negative aerosol RF at the TOA (-2 to -4

223 W m^{-2}) over the Bay of Bengal and the Arabian Sea during spring 2009 - 2013. The clear sky
224 aerosol direct radiative forcing estimated from measurements during the INDOEX
225 experiment (January to March in 1999) over the North Indian Ocean also show similar
226 results (TOA: -7 W m^{-2} , surface: -23 W m^{-2} , and in-atmosphere: $+16 \text{ W m}^{-2}$) (Ramanathan et
227 al., 2001). There is a large variation in the magnitude of RF (at the TOA, surface, and in-
228 atmosphere) reported from observations and our model simulations. This may be due to
229 different regions and different time periods and the relatively coarse model resolution. The
230 observation-based studies attribute positive in-atmospheric radiative forcing to absorbing
231 aerosols (especially black carbon) that lead to a heating of the atmosphere (Rajeev and
232 Ramanathan, 2001; Satheesh et al., 2002).

233 The analysis of the perturbed model experiments indicates that anthropogenic BC
234 aerosols (Fig. 3d-f) have produced a warming at the TOA (Arabian Sea: $1.24 \pm 0.13 \text{ W m}^{-2}$,
235 Bay of Bengal: $1.54 \pm 0.26 \text{ W m}^{-2}$, Indo-Gangetic Plain: $4.33 \pm 0.17 \text{ W m}^{-2}$) and cooling at the
236 surface (Arabian Sea: $-2.56 \pm 0.25 \text{ W m}^{-2}$, Bay of Bengal: $-3.70 \pm 0.49 \text{ W m}^{-2}$, Indo-Gangetic
237 Plain: $-9.27 \pm 0.37 \text{ W m}^{-2}$). OC (Fig. 3g-i) and sulfate (Fig. 3j-l) aerosols have produced
238 significant cooling at the TOA (OC: -0.21 ± 0.13 to $-0.44 \pm 0.15 \text{ W m}^{-2}$; Sulfate: -1.55 ± 0.16 to -
239 $2.14 \pm 0.17 \text{ W m}^{-2}$) and surface (OC: -0.49 ± 0.31 to $-2.56 \pm 0.45 \text{ W m}^{-2}$, Sulfate: -1.19 ± 0.24 to -
240 $2.67 \pm 0.36 \text{ W m}^{-2}$) over the above regions (listed in Table-S1). Figures 3d, 3g, and Fig. 3j
241 further confirm our finding that the positive anomalies of radiative forcing in the Indo-
242 Gangetic plain are due to BC aerosols because of its absorbing property. All the aerosols
243 produce in-atmospheric warming over the Indian region (Fig. 3c, 3f, 3i, 3l) and the North
244 Indian Ocean (Fig. 3c, 3f, 3i). The atmospheric warming over the Arabian Sea and Bay of
245 Bengal is due to BC and OC aerosols with larger contributions by the BC aerosols.

246

247



262 Figure 3: Spatial distribution of net aerosol radiative forcing (CTL - Aerooff) ($W m^{-2}$)
 263 averaged for spring for the years 2001 – 2016 (a) TOA, (b) same as (a) but for surface, (c)
 264 same as (a) but for in-atmosphere (TOA - surface), (d) spatial distribution of radiative forcing
 265 at the TOA (CTL – BCoff) averaged for spring for the years 2001 – 2016, (e) same as (d) but
 266 for surface, (f) same as (d) but for in-atmosphere (TOA - surface), (g) spatial distribution of
 267 radiative forcing at the TOA (CTL - OCoff) averaged for spring during 2001 – 2016, (h)
 268 same as (g) but for surface, (i) same as (h) but for in-atmosphere (TOA - surface), (j) spatial
 269 distribution of radiative forcing at the TOA (CTL - Suloff) averaged for spring during 2001 –
 270 2016, (k) same as (j) but for surface, (l) same as (k) but for in-atmosphere (TOA - surface).
 271 The hatched lines in figure a-l indicate 99% confidence level for the mean differences.

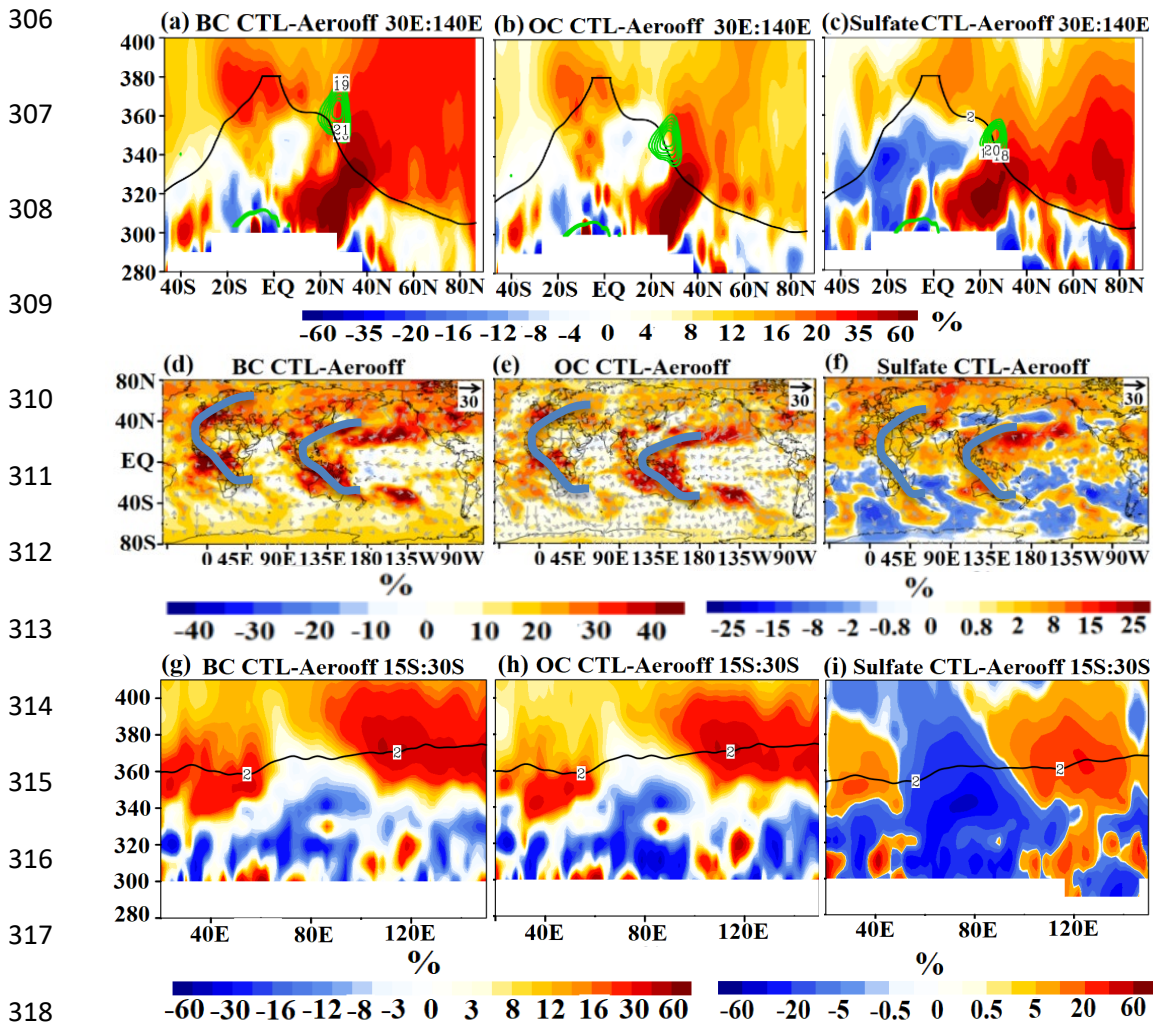
272 3.3. Transport of Asian anthropogenic aerosols into the UTLS

273 Further, we investigate the vertical distribution of aerosols that are transported to the
274 North Indian Ocean. This analysis is performed on the isentropic levels, since past studies
275 show that air mass transport from the troposphere to the stratosphere occurs largely along
276 quasi-isentropic surfaces (Ploeger et al., 2017; Yan et al., 2021). In spring, Asian aerosols are
277 transported partly to the Arabian Sea and Bay of Bengal region and partly to the Western
278 Pacific (Fig. 2a-d). Hence the meridional section is shown over the Indian Ocean and western
279 Pacific region (30° E – 140° E) (Fig. 4 a-c). The vertical distribution of BC, OC, and sulfate
280 aerosols indicates that these aerosols are transported from the boundary layer (10° N – 30° N)
281 into the UTLS (340 – 400K) (Fig. 4a-c and Fig. S2). In the UTLS, at ~ 350 K – 390 K they are
282 transported southward ($\sim 30^{\circ}$ S) and downward (~ 320 K – 340 K). The quasi-isentropic
283 transport occurs via two pathways (1) over Africa (20° E – 60° E) and (2) over the East Indian
284 Ocean and Western-Pacific (95° E – 140° E) (Fig. 4d-f). The downward penetration of
285 aerosols (BC, OC, and sulfate) in the Southern Hemisphere (15° S – 30° S) to 320 K – 340 K
286 via the above mentioned two pathways is also evident in Figure 4 g-i.

287 In the following, we further explore processes responsible for inter-hemispheric transport.
288 Our analysis indicates that the Hadley circulation (Fig. 5a and Fig. S3) with its ascending
289 branch over the Indian Ocean and adjoining region (60° E – 140° E, 0 – 30° N), lifts the South
290 Asian aerosols to the UTLS. These aerosols enter the westerly jet (Fig. 4 d-f).

291 The distribution of zonal winds in Fig. 5b shows transport into the southern hemisphere
292 preferentially in regions of equatorial westerly winds, so-called "westerly duct" regions
293 (Vaugh and Polvani, 2000; Yan et al., 2021), where Rossby-wave breaking occurs (Fig. 5b
294 and Fig. S4). This is consistent with findings from Frederiksen et al. (2018) who have also
295 shown interhemispheric transport of CO_2 via Pacific and Atlantic westerly ducts during the

296 spring season. Fig. 5c shows that changes in South Asian aerosols concentrations cause a
 297 shift in the Pacific duct. Thus interhemispheric transport occurs through (1) an Atlantic duct
 298 and (2) a slightly shifted Pacific duct ($5^{\circ} \text{S} - 5^{\circ} \text{N}$, $50^{\circ} \text{E} - 140^{\circ} \text{E}$), i.e. over the Indian-
 299 Ocean-Western Pacific region (also see Fig. 4 d-f). The shift in Pacific duct in a response to
 300 South Asian aerosol changes is likely due to higher Rossby wave bearing near south Asia.
 301 The geopotential (Fig 5d) and potential vorticity (Fig. S5) anomalies (CTL-Aerooff) show
 302 Rossby wave breaking near the Indian-Ocean-Western Pacific region that could lead to
 303 Southern hemispheric transport through the Indian-Ocean-Western Pacific region path (Fig 5
 304 c-d). In addition, the interhemispheric transport is also likely influenced by the monthly
 305 migration and the strength of the Hadley circulation (Fig. S3).



319 Figure 4: Meridional cross-section over Indian Ocean-western Pacific (averaged 30° E –
 320 140° E and for the spring season for the years 2001 – 2016) of anomalies (%) (CTL-
 321 Aerooff) of (a-c) BC, OC, and sulfate aerosols. Green contours in (a-c) indicate westerly jet.
 322 Fig (d-f) spatial distribution of BC, OC and Sulfate aerosols averaged at 360 – 390K
 323 isentropic levels and the spring season for the years 2001 – 2016, vectors in Figs. d-f
 324 indicate anomalies of winds (m s^{-1}). (g-i) Zonal cross-section (averaged over 15° S – 30° S
 325 and for the spring season for the years 2001 – 2016) and for the spring season for BC, OC,
 326 and sulfate aerosols. The black line of 2 PV (in a-c and g-i) indicates the dynamical
 327 tropopause.

328

329

330

331

332

333

334

335

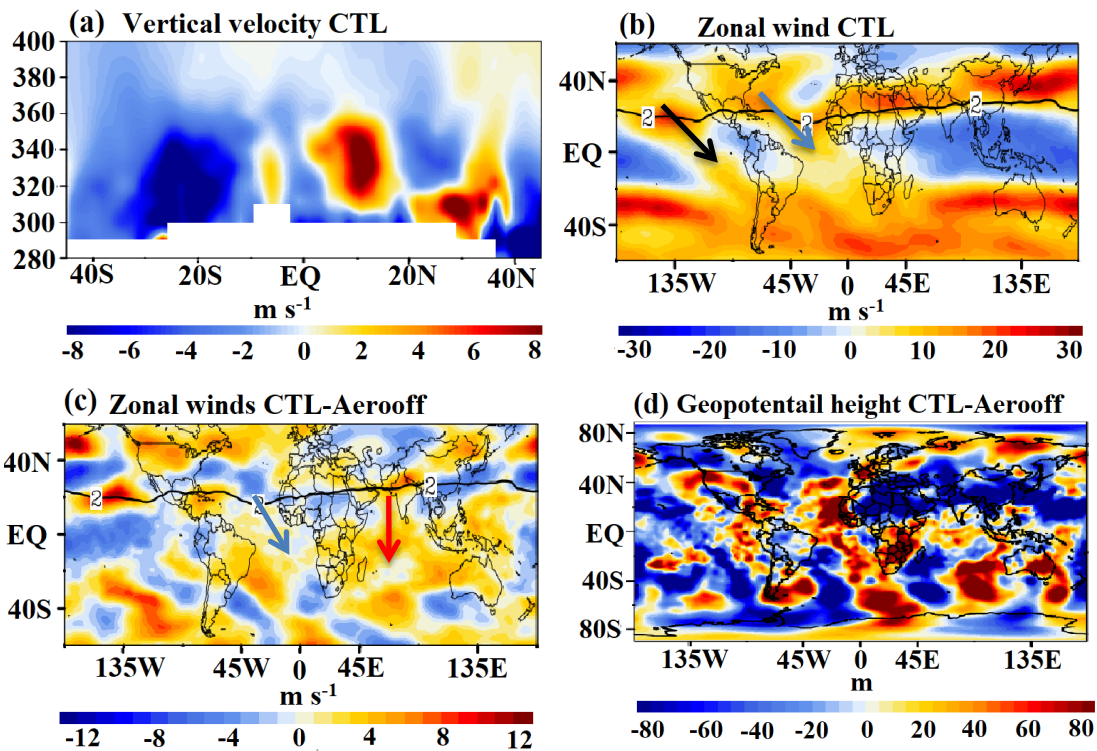
336

337

338

339

340



341 Figure 5: Meridional cross section of vertical velocities (m s^{-1}) (averaged for 65° E – 140° E
 342 and for spring season during 2001 – 2016). Vertical velocities are scaled by 300, (b) zonal
 343 winds at 360 K isentropic level from CTL simulations, a black arrow indicates Pacific duct
 344 and blue arrow indicates Atlantic duct, (c) anomalies (CTL-Aerooff) zonal winds at 360 K
 345 isentropic level. A blue arrow indicates the Atlantic duct and red arrow indicates duct over
 346 the Indian Ocean, (d) anomalies (CTL-Aerooff) of geopotential height (m) at the 340K
 347 potential temperature level. The potential vorticity (2 PVU) is indicated by the black contour
 348 in Figs. b-c.

349

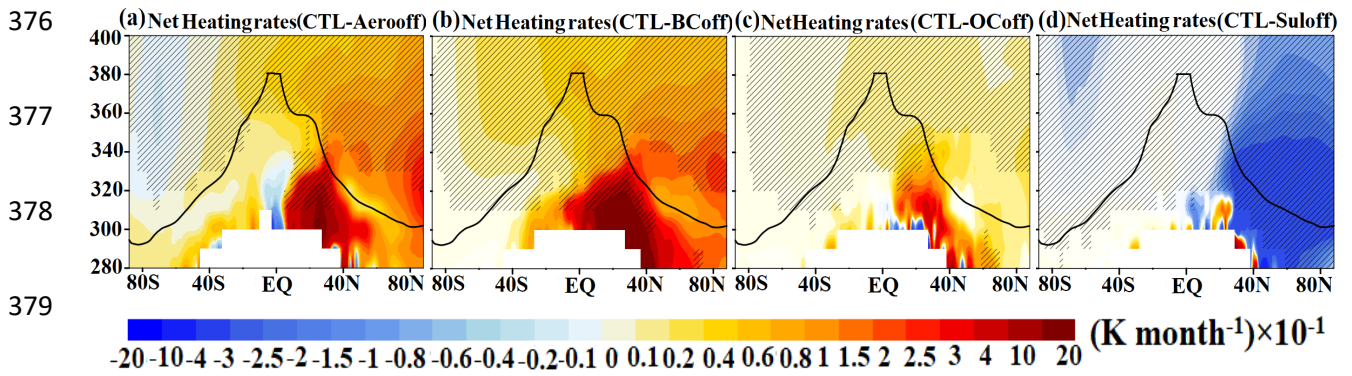
350 Further, in the UTLS, South Asian aerosols are transported to the Arctic (Fig. 4 a-c). There is
 351 an aerosol enhancement in the Arctic (BC: 10 to 30 %, OC: 10 to 20 %, Sulfate: 5 to 30 %).

352 Our analysis shows that transport to the Arctic occurs every year in the UTLS which causes
353 heating in the lower stratosphere (380 K – 400K) (see Section 3.4).

354 **3.4. Impacts on the net heating rate and water vapour**

355 Carbonaceous aerosols absorb solar radiation, leading to atmospheric heating, while
356 predominately scattering aerosols such as sulfate reflect and scatter back solar radiation,
357 therefore cooling the atmosphere below (Fadnavis et al., 2019). Here, we analyse net heating
358 rates (short wave + long wave) induced by all the anthropogenic Asian aerosols (CTL -
359 Aerooff). Changes in the net heating rates are induced by the aerosol changes; any changes in
360 dynamical heating will be intrinsic. The vertical distribution of net heating rate anomalies
361 over the North Indian Ocean and Western Pacific region (30° E – 140° E) indicates increase
362 in heating rates in the region of elevated anthropogenic aerosols in the troposphere (0.15 to
363 0.4 K month⁻¹, 5 – 60 %) and UTLS (0.02 to 0.3 K month⁻¹, 10 – 60 %) (Fig. 6a-d, Fig. 4, and
364 Fig. S2). Heating rate anomalies estimated over the North Indian Ocean and western Pacific
365 region from BC (CTL - BCoff), OC (CTL - OCoff), and Sulfate (CTL - Suloff) show that BC
366 and OC aerosols produce heating in the troposphere (280K – 340K) (10° N – 40° N) (BC:
367 0.6 to 2 K month⁻¹, 10 – 50% , OC: 0.2 to 0.4 K month⁻¹, 0.5 – 4 %) and UTLS over Northern
368 hemisphere (BC: 0.08 to 0.2 K month⁻¹, 30 – 45%, OC: 0.02 to 0.06 K month⁻¹, 0.2 – 1.5 %),
369 while sulfate aerosols produce atmospheric cooling in the troposphere and UTLS -0.02 to -
370 0.4 K month⁻¹ (5 – 40 %) (280 - 400K) (Fig. 6a-d). Black carbon aerosol produces higher
371 heating than organic carbon aerosols. The shortwave heating due to BC aerosols is the major
372 contributor to the total heating. In general, these aerosols increase heating in the troposphere
373 extending to the lower stratosphere (400K) over the South Asian region (Fig. 6a). There is
374 enhancement in heating rates along the path of aerosols transported to the Arctic.

375



381 Figure 6: Meridional cross-section of heating rates (K month⁻¹) over the Indian Ocean-
 382 western Pacific (averaged 30° E – 140° E and for the spring season for the years 2001 – 2016)
 383 (a) from CTL - Aerooff simulation, (b) same (a) but from CTL - BCoff simulation (c) same
 384 (a) but from CTL - OCoff simulation, (d) same (a) but from CTL - Suloff simulation. Hatches
 385 in Figs. a-d indicate 95% significance level. A black line in Figs. a-d indicates the dynamical
 386 tropopause.

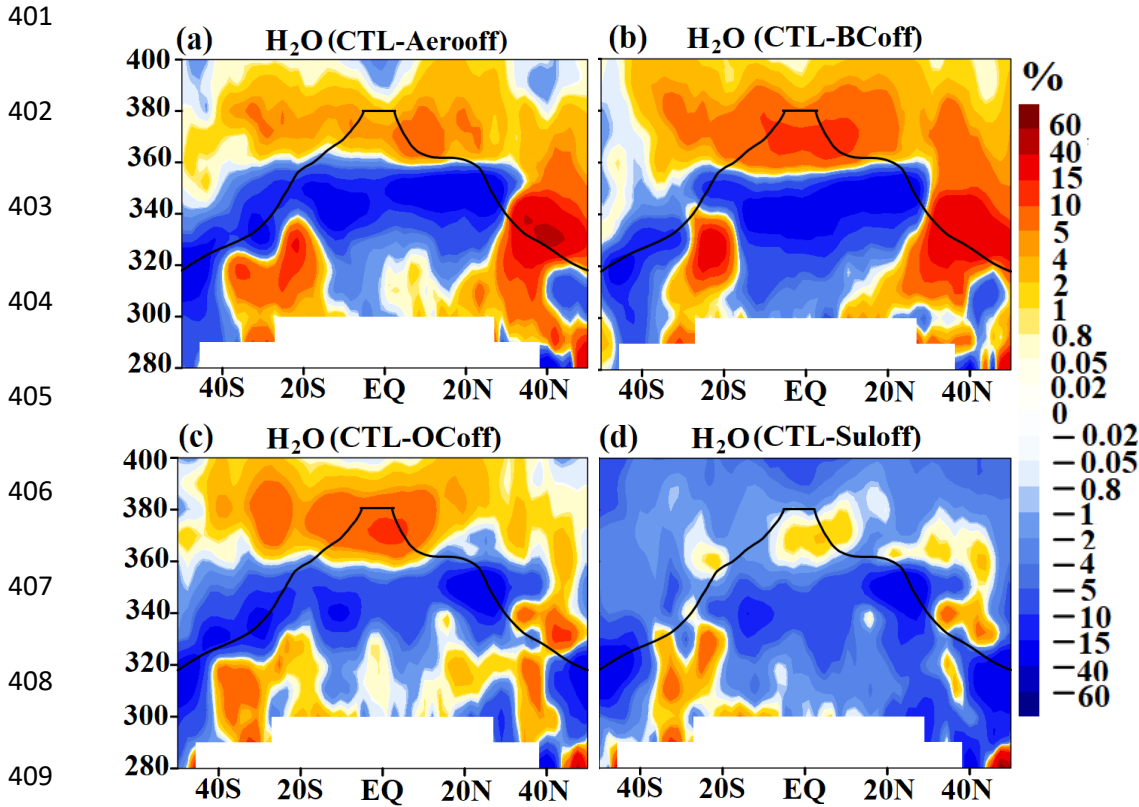
387

388 The vertical distribution of water vapor over the Indian Ocean-Western Pacific region (30°
 389 E – 140° E) (CTL - Aerooff) shows that water vapour concentrations are enhanced by 1-10%
 390 along the path of elevated aerosols (Fig. 7a and Fig. 4). In the UTLS, water vapour is
 391 transported to the southern hemisphere ~45° S. This may be due to heating caused by the
 392 Asian aerosols. The impact of BC (CTL - BCoff), OC (CTL - OCoff), and Sulfate (CTL -
 393 Suloff) on the water vapor distribution (Fig. 7 b-d) shows that BC aerosols play a major role
 394 in water vapor enhancement in the UTLS (Fig. 7 b). Water vapor enhancement by BC
 395 aerosols over the Indian Ocean-Western Pacific region is ~ 1 – 15 % (Fig. 7b). The water
 396 vapor enhancement by OC aerosols in the UTLS region is 0.8 – 15% (Fig. 7c) and by sulfate
 397 aerosols ~0.2 – 1% in pockets (Fig. 7d).

398

399

400

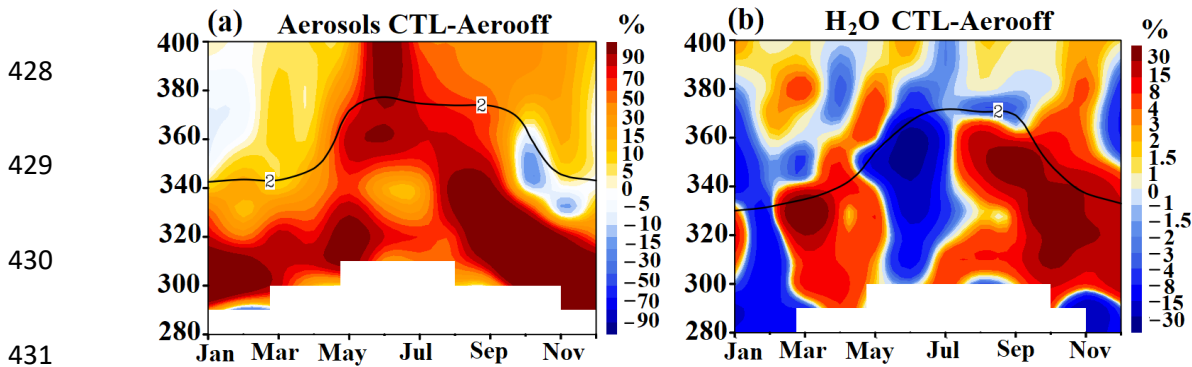


410 Figure 7: (a) Meridional cross-section over the Indian Ocean-western Pacific (averaged over
 411 $30^{\circ} \text{ E} - 140^{\circ} \text{ E}$) of anomalies of water vapour (%) (CTL - Aerooff) the for spring season for
 412 the years 2001 – 2016, (b) same as (a) but from CTL - BCoff simulations, (c) same as (a) but
 413 from CTL - OCoff simulations, (d) same as (a) but from CTL - Suloff simulations. A black
 414 line in Figs. a-d indicates the dynamical tropopause.

415

416 Although the focus of the manuscript is on the transport of aerosols during the spring season,
 417 it should be noted that the anthropogenic South Asian aerosols are also transported to the
 418 UTLS during the monsoon season (Shindell et al., 2008, Fadnavis et al., 2013, 2017, 2019,
 419 Zheng et al., 2021). Annual distribution anomalies of aerosols (average of BC, OC, and
 420 sulfate) show the transport of aerosols into the UTLS during the spring and monsoon seasons
 421 (April to September) from South Asian region (Fig. 8a). In the lower stratosphere, these
 422 aerosols persist for a few months (Fig. 8a) thus their effect will be seen for an extended time.
 423 These aerosols enhance tropospheric heating thereby transporting elevated water vapour into
 424 the lower stratosphere (Fig. 8b). Figure 8a also shows the transport of aerosols into the lower
 425 stratosphere during spring and the monsoon seasons (March-September). The aerosol induced

426 enhanced water vapour also shows enhancement in the lower stratosphere during the same
 427 time (Fig. 8b).



432 Figure 8: (a) Annual distribution of anomalies of aerosols (CTL - Aerooff) (averaged of BC,
 433 OC and sulfate aerosols) (%) averaged South Asian region (50° E – 100° E, 20° N – 40° N),
 434 (b) same as (a) but for water vapour (%) over North Indian-Ocean-Western-Pacific (30° E –
 435 140° E, 20° N – 40° N). A black line in Figs. a-b indicates the dynamical tropopause.

436

437 Further, we analyze the correlation between heating rates and carbonaceous aerosol
 438 amounts in the UTLS (380 K level) in the Arctic during 2001 – 2016 (spring mean) (Fig. 9)
 439 from Aerooff, BCoff, and OCoff in comparison with CTL simulations. The carbonaceous
 440 aerosols show a positive correlation (correlation coefficient r : 0.55 to 0.85) with the UTLS
 441 heating rates indicating that transported carbonaceous aerosols enhance UTLS heating in the
 442 Arctic. It should be noted that increase in aerosols at the Arctic also occurs during the
 443 monsoon season (Fadnavis et al., 2017a, 2017b, 2019, Zheng et al., 2021) which may affect
 444 the dynamics and aerosol amounts in the spring of the next year in the UTLS.

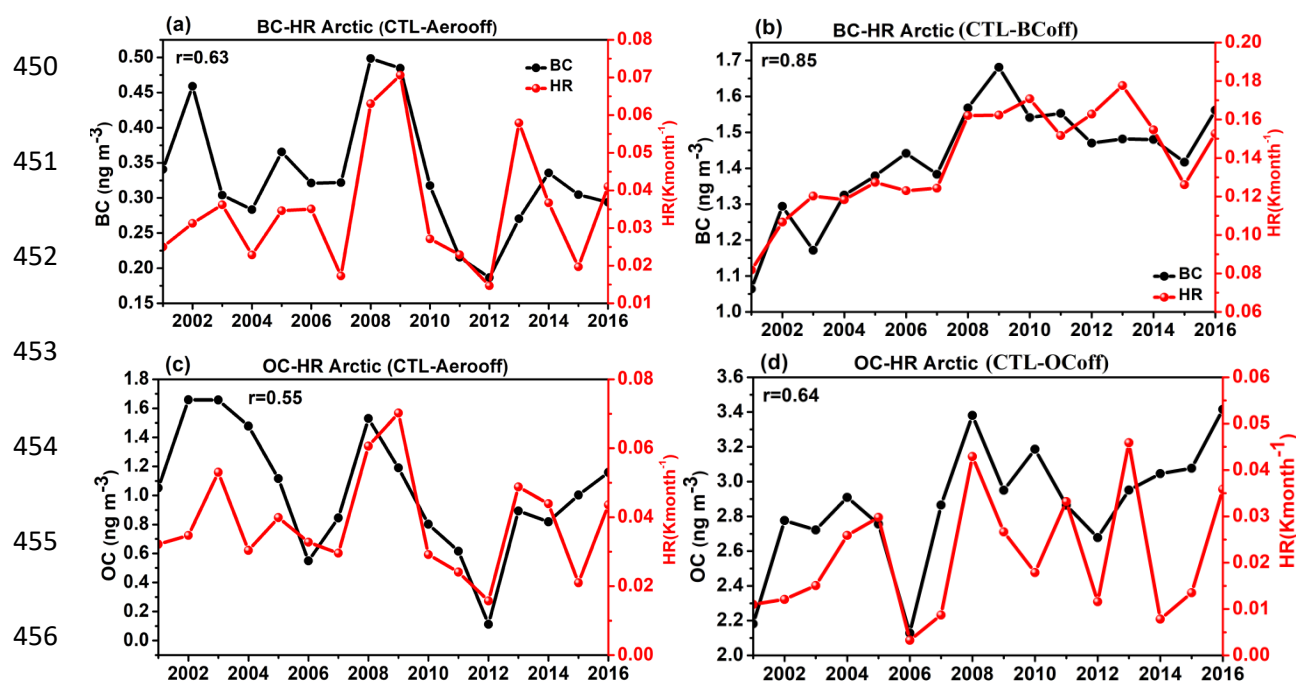
445

446

447

448

449



457 Figure 9: (a) Time series of BC aerosols and heating rates averaged for spring in the UTLS
 458 (380 K) in the Arctic (65° N – 85° N, $0 - 360^{\circ}$) (from CTL – Aerooff), (b) same as (a) but
 459 from CTL – BCoff. (c) same as (a) but for OC, (d) same as (c) but form CTL – OCoff. The
 460 correlation coefficient (r) between anomalies of BC/OC aerosols and heating rates is
 461 indicated in panels a-d.

462

463 Importantly, South Asian aerosols enhance water vapor in the lower stratosphere in the
 464 tropical and subtropical latitudes (45° S – 45° N). Water vapor being a greenhouse gas further
 465 enhances the heating of the troposphere leading to a positive feedback. The increase in water
 466 vapor in the stratosphere also warms the Earth's surface (Shindell, 2001; Solomon et al.,
 467 2010). Solomon et al. (2010) estimated that an increase in the stratospheric water vapor by 1
 468 ppmv accounts for 0.24 W m^{-2} radiative forcing at the TOA. The SABER and MLS
 469 observations showed an increase in stratospheric water vapor by 0.45 ppmv globally during
 470 2003 – 2017 (Yue et al., 2019). Thus the radiative forcing due to water vapor increase ($0.02 -$
 471 0.14 ppmv) in response to South Asian anthropogenic aerosols is not negligible for surface
 472 warming globally. Further, increasing stratospheric water vapour could also lead to ozone
 473 depletion (e.g., Shindell, 2001, Robrecht et al., 2019).

474

475 **4. Conclusions**

476 A series of ECHAM6-HAMMOZ chemistry-climate simulations for South Asian
477 anthropogenic aerosols were used to understand the transport pathways of South Asian
478 aerosols in spring and their impacts on the UTLS. The model simulations show that large
479 amounts of South Asian aerosols are transported during spring to the Arabian Sea (increases
480 in AOD by: 0.02 – 0.12 from CTL - Aerooff) and Bay of Bengal (increases in AOD by: 0.16
481 to 0.8 from CTL - Aerooff) and Western Pacific (increases in AOD by 0.08 to 0.18). These
482 aerosols are further lifted up into the UTLS from the North Indian Ocean and South Asia (10°
483 N – 30° N). In the UTLS, they are also transported to the southern hemisphere (15° S – 30°
484 S) and downward (320K – 340K). The processes responsible for interhemispheric transport
485 are as follows:

486 (1) South Asian aerosols are lifted up to the UTLS by the ascending branch of Hadley
487 circulation. In the UTLS the aerosols enter the westerly Jet.

488 (2) They are transported to the Southern hemisphere via the Atlantic westerly duct (5° S – 5°
489 N, 10° W – 40° W) and Pacific westerly duct (5° S – 5° N, 50° E – 140° E),

490 (3) A shift in the Pacific westerly duct may be due to an increase in Rossby Wave Breaking
491 over the north Indian Ocean-western Pacific induced by South Asian aerosols.

492 The anthropogenic aerosol produces significant radiative impacts over the Indo-Gangetic
493 Plain (RF anomalies estimated from CTL-Aerooff simulations, TOA: $+1.27 \pm 0.16 \text{ W m}^{-2}$,
494 Surface: $-11.16 \pm 0.50 \text{ W m}^{-2}$, In-atmosphere: $+12.44 \pm 0.42 \text{ W m}^{-2}$) and the Arabian Sea (RF at
495 the TOA: $-0.72 \pm 0.14 \text{ W m}^{-2}$, surface: $-3.00 \pm 0.28 \text{ W m}^{-2}$, In-atmosphere: $+2.27 \pm 0.19 \text{ W m}^{-2}$).
496 Interestingly, RF at the TOA over the Indo-Gangetic Plain is positive ($+4.33 \pm 0.17 \text{ W m}^{-2}$)
497 due to the emission of BC aerosols alone. The anthropogenic aerosols enhance heating in the

498 troposphere over the North Indian Ocean (estimated from CTL-Aerooff) by 0.15 to 0.4 K
499 month⁻¹ (4 – 60 %) and UTLS by 0.02 to 0.3 K month⁻¹ (10 – 60 %).

500 The heating of the troposphere by the carbonaceous aerosol (mainly BC) increases
501 temperature and thereby tropospheric water vapor amounts over the North Indian Ocean and
502 adjoining regions. The elevated water vapor is transported to the UTLS from the North Indian
503 ocean-western Pacific region (30° E – 140° E, 20° N – 40° N). In the UTLS it is transported
504 to the Southern Hemisphere ~45° S. BC aerosols play a major role in water vapor
505 enhancement in the lower stratosphere (increased water vapor by 0.8 – 5 %). As water vapour
506 is a greenhouse gas, this enhancement of stratospheric water vapour could potentially amplify
507 the warming of the troposphere and surface and cause a positive feedback (e.g. Shindell,
508 2001; Solomon et al., 2010).

509 *Acknowledgments:* The authors thank the staff of the High Power Computing Centre (HPC)
510 in the Indian Institute of Tropical Meteorology, Pune, India, Pune, India. We thank the
511 reviewers for their valuable suggestions. We thank Jonathon Wright for useful discussions
512 and suggestions that improved the quality of the manuscript.

513 **Data availability:** The data used in this study are generated from ECHAM6-HAMMOZ
514 model simulations at the High-performance computing system in the Indian Institute of
515 Tropical Meteorology, Pune, India. The AOD data from MODIS Terra used here can be
516 downloaded from <https://ladsweb.modaps.eosdis.nasa.gov/archive/allData/61/MODATML2/>,
517 and MISR from <https://misr.jpl.nasa.gov/getData/accessData/>.

518

519 **Author contributions:** S. F. initiated the idea. A. J., S. S., A. A., performed model analysis.
520 R. M., and A. R. contributed to analysis and study design. All authors contributed to the
521 writing and discussions of the manuscript.

522 **Competing Interests:** Some authors are members of the editorial board of Atmospheric
523 Chemistry and Physics. The peer-review process was guided by an independent editor, and
524 the authors have also no other competing interests to declare.

525

526 **References:**

- 527 Aswini, A. R., Hegde, P., Aryasree, S., Girach, I. A. and Nair, P. R.: Continental outflow of
528 anthropogenic aerosols over Arabian Sea and Indian Ocean during wintertime: ICARB-
529 2018 campaign, *Sci. Total Environ.*, 712, 135214, doi:10.1016/j.scitotenv.2019.135214,
530 2020.
- 531 Babu, S. S., Manoj, M. R., Moorthy, K. K., Gogoi, M. M., Nair, V. S., Kompalli, S. K.,
532 Satheesh, S. K., Niranjana, K., Ramagopal, K., Bhuyan, P. K. and Singh, D.: Trends in
533 aerosol optical depth over Indian region: Potential causes and impact indicators, *J.*
534 *Geophys. Res. Atmos.*, 118, 11,794-11,806, doi:10.1002/2013JD020507, 2013.
- 535 Budhavant, K., Bikkina, S., Andersson, A., Asmi, E., Backman, J., Kesti, J., Zahid, H.,
536 Satheesh, S. K. and Gustafsson, Ö.: Anthropogenic fine aerosols dominate the
537 wintertime regime over the northern Indian Ocean, *Tellus, Ser. B Chem. Phys.*
538 *Meteorol.*, 70, 1–15, doi:10.1080/16000889.2018.1464871, 2018.
- 539 Chavan, P., Fadnavis, S., Chakroborty, T., Sioris, C. E. and Müller, R.: The outflow of Asian
540 biomass burning carbonaceous aerosol into the UTLS in spring: Radiative effects seen
541 in a global model, 21, 14371–14384, <https://doi.org/10.5194/acp-2021-494>, 2021.
- 542 Corrigan, C. E., Roberts, G. C., Ramana, M. V., Kim, D. and Ramanathan, V.: Capturing
543 vertical profiles of aerosols and black carbon over the Indian Ocean using autonomous
544 unmanned aerial vehicles, *Atmos. Chem. Phys.*, 8, 737–747, doi:10.5194/acp-8-737-
545 2008, 2008.
- 546 Collins, M., Sutherland, M., Bouwer, L., Cheong, S.-M., Frölicher, T. L., Jacot Des Combes,
547 H., Roxy, M. K., Losada, I., McInnes, K. L., Ratter, B., Rivera-Arriaga, E., Susanto, R.
548 D., Swingedouw, D., Tibig, L., Bakker, P., Eakin, C. M., Emanuel, K., Grose, M.,
549 Hemer, M., Jackson, L., Kääh, A., Kajtar, J. B., Knutson, T., Laufkötter, C., Noy, I.,

550 Payne, M., Ranasinghe, R., Sgubin, G. and Timmermans, M.-L.: Extremes, Abrupt
551 Changes and Managing Risks, IPCC Spec. Rep. Ocean Cryosph. a Chang. Clim., 589–
552 655, 2019.

553 De Reus, M., Krejci, R., Williams, J., Fischer, H., Scheele, R. and Ström, J.: Vertical and
554 horizontal distributions of the aerosol number concentration and size distribution over
555 the northern Indian Ocean, *J. Geophys. Res. Atmos.*, 106, 28629–28641,
556 doi:10.1029/2001JD900017, 2001.

557 Dickerson, R. R., Andreae, M. O., Campos, T., Mayol-Bracero, O. L., Neusuess, C. and
558 Streets, D. G.: Analysis of black carbon and carbon monoxide observed over the Indian
559 Ocean: Implications for emissions and photochemistry, *J. Geophys. Res. Atmos.*, 107,
560 doi:10.1029/2001JD000501, 2002.

561 Fadnavis, S., Kalita, G., Rowlinson, M., Rap, A., Li, J.-L. F., Gasparini, B., Laakso, A. and
562 Müller, R.: The impact of increases in South Asian anthropogenic emissions of SO₂ on
563 sulfate loading in the upper troposphere and lower stratosphere during the monsoon
564 season and the associated radiative changes, *Atmos. Chem. Phys.*, 19, 9989–10008,
565 <https://doi.org/10.5194/acp-19-9989-2019>, 2019.

566 Fadnavis, S., Roy, C., Sabin, T. P., Ayantika, D. C. and Ashok, K.: Potential modulations of
567 pre-monsoon aerosols during El Niño: impact on Indian summer monsoon, *Clim. Dyn.*,
568 49, 2279–2290, doi:10.1007/s00382-016-3451-6, 2017a.

569 Fadnavis, S., Kalita, G., Ravi Kumar, K., Gasparini, B. and Li, J. L. F.: Potential impact of
570 carbonaceous aerosol on the upper troposphere and lower stratosphere (UTLS) and
571 precipitation during Asian summer monsoon in a global model simulation, *Atmos.*
572 *Chem. Phys.*, 17, 11637–11654, doi:10.5194/acp-17-11637-2017, 2017b.

573 Fadnavis, S. and Chattopadhyay, R.: Linkages of subtropical stratospheric intraseasonal

574 intrusions with Indian summer monsoon deficit rainfall, *J. Clim.*, 30, 5083–5095,
575 doi:10.1175/JCLI-D-16-0463.1, 2017.

576 Fadnavis, S., Semeniuk, K., Pozzoli, L., Schultz, M. G., Ghude, S. D., Das, S. and Kakatkar,
577 R.: Transport of aerosols into the UTLS and their impact on the asian monsoon region
578 as seen in a global model simulation, *Atmos. Chem. Phys.*, 13, 8771–8786,
579 doi:10.5194/acp-13-8771-2013, 2013.

580 Fadnavis, S., Sabin, T. P., Rap, A., Müller, R., Kubin, A. and Heinold, B.: The impact of
581 COVID-19 lockdown measures on the Indian summer monsoon, *Environ. Res. Lett.*,
582 16, 074054, doi:10.1088/1748-9326/ac109c, 2021a.

583 Fadnavis S., Müller R , Chakraborty T. , Sabin T. P., Laakso A. , Rap A. , Griessbach S.,
584 Vernier J-P., and Tilmes S., The role of tropical volcanic eruptions in exacerbating
585 Indian droughts, *Sci. Rep.*, 11, 2714, doi.org/10.1038/s41598-021-81566-0, 2021b.

586 Frederiksen, J. S. and Francey, R. J.: Unprecedented strength of Hadley circulation in 2015–
587 2016 impactson CO2 interhemispheric difference, *Atmos. Chem. Phys.*, 18, 14837–
588 14850, <https://doi.org/10.5194/acp-18-14837-2018>, 2018.

589 Holton, J. R., Haynes, P. H., McIntyre, M. E., Douglass, A. R., Rood, R. B., Pfister, L.:
590 Stratosphere-troposphere exchange, *Reviews of Geophysics*, 33, 403-439,
591 <https://doi.org/10.1029/95RG02097>, 1995.

592 Jose, S., Nair, V. S. and Babu, S. S.: Anthropogenic emissions from South Asia reverses the
593 aerosol indirect effect over the northern Indian Ocean, *Sci. Rep.*, 10, 18360,
594 doi:10.1038/s41598-020-74897-x, 2020.

595 Karambelas, A., Holloway, T., Kinney, P. L., Fiore, A. M., Defries, R., Kieseewetter, G. and
596 Heyes, C.: Urban versus rural health impacts attributable to PM2.5 and O₃ in northern
597 India, *Environ. Res. Lett.*, 13, 064010, doi:10.1088/1748-9326/aac24d, 2018.

598 Kahn, R. A., Garay, M. J., Nelson, D. L., Yau, K. K., Bull, M. A., Gaitley, B. J., Martonchik,
599 J. V., and Levy, R. C.: Satellite-derived aerosol optical depth over dark water from
600 MISR and MODIS: Comparisons with AERONET and implications for climatological
601 studies, *J. Geophys. Res.*, 112, D18205, doi:10.1029/2006JD008175, 2007.

602 Kunz, A., Konopka, P., Müller, R. and Pan, L. L.: The dynamical tropopause based on
603 isentropic potential vorticity gradients *J. Geophys. Res.*, 116, D01110,
604 doi:10.1029/2010JD014343, 2011.

605 Lu, Z., Zhang, Q. and Streets, D. G.: Sulfur dioxide and primary carbonaceous aerosol
606 emissions in China and India, 1996-2010, *Atmos. Chem. Phys.*, 11, 9839–9864,
607 doi:10.5194/acp-11-9839-2011, 2011.

608 Mahowald, N. M., Hamilton, D. S., Mackey, K. R. M., Moore, J. K., Baker, A. R., Scanza, R.
609 A. and Zhang, Y.: Aerosol trace metal leaching and impacts on marine microorganisms,
610 *Nat. Commun.*, 9, 2614, doi:10.1038/s41467-018-04970-7, 2018.

611 Mayol-Bracero, O. L., Gabriel, R., Andreae, M. O., Kirchstetter, T. W., Novakov, T., Ogren,
612 J., Sheridan, P. and Streets, D. G.: Carbonaceous aerosols over the Indian Ocean during
613 the Indian Ocean Experiment (INDOEX): Chemical characterization, optical properties,
614 and probable sources, *J. Geophys. Res. Atmos.*, 107, 8030,
615 doi:10.1029/2000JD000039, 2002.

616 McFarquhar, G. M. and Wang, H.: Effects of aerosols on trade wind cumuli over the Indian
617 Ocean: Model simulations, *Q. J. R. Meteorol. Soc.*, 132, 821–843,
618 doi:10.1256/qj.04.179, 2006.

619 Meehl, G. A., Arblaster, J. M. and Collins, W. D.: Effects of black carbon aerosols on the
620 Indian monsoon, *J. Clim.*, 21, 2869–2882, doi:10.1175/2007JCLI1777.1, 2008.

621 Nair, V. S., Babu, S. S., Manoj, M. R., Moorthy, K. K. and Chin, M.: Direct radiative effects
622 of aerosols over South Asia from observations and modeling, *Clim. Dyn.*, 49, 1411–
623 1428, doi:10.1007/s00382-016-3384-0, 2017.

624 Neubauer, D., Lohmann, U., Hoose, C. and Frontoso, M. G.: Impact of the representation of
625 marine stratocumulus clouds on the anthropogenic aerosol effect, *Atmos. Chem. Phys.*,
626 14, 11997–12022, doi:10.5194/acp-14-11997-2014, 2014.

627 Paliwal, U., Sharma, M. and Burkhart, J. F.: Monthly and spatially resolved black carbon
628 emission inventory of India: Uncertainty analysis, *Atmos. Chem. Phys.*, 16, 12457–
629 12476, doi:10.5194/acp-16-12457-2016, 2016.

630 Papaspiropoulos, G., Martinsson, B. G., Zahn, A., Brenninkmeijer, C. A. M., Hermann, M.,
631 Heintzenberg, J., Fischer, H. and Van Velthoven, P. F. J.: Aerosol elemental
632 concentrations in the tropopause region from intercontinental flights with the Civil
633 Aircraft for Regular Investigation of the Atmosphere Based on an Instrument Container
634 (CARIBIC) platform, *J. Geophys. Res. Atmos.*, 107, 4671, doi:10.1029/2002JD002344,
635 2002.

636 Pathak, H. S., Satheesh, S. K., Moorthy, K. K. and Nanjundiah, R. S.: Assessment of regional
637 aerosol radiative effects under the SWAAMI campaign - Part 2: Clear-sky direct
638 shortwave radiative forcing using multi-year assimilated data over the Indian
639 subcontinent, *Atmos. Chem. Phys.*, 20, 14237–14252, doi:10.5194/acp-20-14237-2020,
640 2020.

641 Penner, J. E., Chuang, C. C. and Grant, K.: Climate forcing by carbonaceous and sulfate
642 aerosols, *Clim. Dyn.*, 14, 839–851, doi:10.1007/s003820050259, 1998.

643 Ploeger, F., Konopka, P., Walker, K., and Riese, M.: Quantifying pollution transport from the
644 Asian monsoon anticyclone into the lower stratosphere, *Atmos. Chem. Phys.*, 17, 7055–

645 7066, <https://doi.org/10.5194/acp-17-7055-2017>, 2017.

646 Rajeev, K. and Ramanathan, V.: Direct observations of clear-sky aerosol radiative forcing
647 from space during the Indian Ocean Experiment, *J. Geophys. Res. Atmos.*, 106, 17221–
648 17235, doi:10.1029/2000JD900723, 2001.

649 Ramachandran, S., Rupakheti, M. and Lawrence, M. G.: Aerosol-induced atmospheric
650 heating rate decreases over South and East Asia as a result of changing content and
651 composition, *Sci. Rep.*, 10, 20091, doi:10.1038/s41598-020-76936-z, 2020a.

652 Ramachandran, S., Rupakheti, M. and Lawrence, M. G.: Black carbon dominates the aerosol
653 absorption over the Indo-Gangetic Plain and the Himalayan foothills, *Environ. Int.*,
654 142, 105814, doi:10.1016/j.envint.2020.105814, 2020b.

655 Ramanathan, V., Chung, C., Kim, D., Bettge, T., Buja, L., Kiehl, J. T., Washington, W. M.,
656 Fu, Q., Sikka, D. R. and Wild, M.: Atmospheric brown clouds: Impacts on South Asian
657 climate and hydrological cycle, *Proc. Natl. Acad. Sci. U. S. A.*, 102, 5326–5333,
658 doi:10.1073/pnas.0500656102, 2005.

659 Ramanathan, V., Crutzen, P. J., Lelieveld, J., Mitra, A. P., Althausen, D., Anderson, J.,
660 Andreae, M. O., Cantrell, W., Cass, G. R., Chung, C. E., Clarke, A. D., Coakley, J. A.,
661 Collins, W. D., Conant, W. C., Dulac, F., Heintzenberg, J., Heymsfield, A. J., Holben,
662 B., Howell, S., Hudson, J., Jayaraman, A., Kiehl, J. T., Krishnamurti, T. N., Lubin, D.,
663 McFarquhar, G., Novakov, T., Ogren, J. A., Podgorny, I. A., Prather, K., Priestley, K.,
664 Prospero, J. M., Quinn, P. K., Rajeev, K., Rasch, P., Rupert, S., Sadourny, R., Satheesh,
665 S. K., Shaw, G. E., Sheridan, P. and Valero, F. P. J.: Indian Ocean Experiment: An
666 integrated analysis of the climate forcing and effects of the great Indo-Asian haze, *J.*
667 *Geophys. Res. Atmos.*, 106, 28371–28398, doi:10.1029/2001JD900133, 2001.

668 Robrecht, S., Vogel, B., Grooß, J.-U., Rosenlof, K., Thornberry, T., Rollins, A., Krämer, M.,

669 Christensen, L. and Müller, R.: Mechanism of ozone loss under enhanced water vapour
670 conditions in the mid-latitude lower stratosphere in summer, *Atmos. Chem. Phys.*, 19,
671 5805–5833, doi:10.5194/acp-19-5805-2019, 2019.

672 Romatschke, U. and Houze, R. A.: Characteristics of precipitating convective systems in the
673 South Asian monsoon, *J. Hydrometeorol.*, 12, 3–26, doi:10.1175/2010JHM1289.1,
674 2011.

675 Satheesh, S. K., Ramanathan, V., Holben, B. N., Krishna Moorthy, K., Loeb, N. G., Mating,
676 H., Prospero, J. M. and Savoie, D.: Chemical, microphysical, and radiative effects of
677 Indian Ocean aerosols, *J. Geophys. Res.*, 107, 4725, doi:10.1029/2002JD002463, 2002.

678 Satheesh, S. K. and Ramanathan, V.: Large differences in tropical aerosol forcing at the top
679 of the atmosphere and Earth’s surface, *Nature*, 405, 60–63, doi:10.1038/35011039,
680 2000.

681 Shindell, D. T.: Climate and ozone response to increased stratospheric water vapor, *Geophys.*
682 *Res. Lett.*, 28, 1551–1554, doi:10.1029/1999GL011197, 2001.

683 Solomon, S., Rosenlof, K. H., Portmann, R. W., Daniel, J. S., Davis, S. M., Sanford, T. J. and
684 Plattner G. K.: Contributions of stratospheric water vapor to decadal changes in the rate
685 of global warming, *Science*, 327, 1219–1223, 0.1126/science.1182488, 2010.

686 Shindell, D. T., Chin, M., Dentener, F., Doherty, R. M., Faluvegi, G., Fiore, A. M., Hess, P.,
687 Koch, D. M., MacKenzie, I. A., Sanderson, M. G., Schultz, M. G., Schulz, M.,
688 Stevenson, D. S., Teich, H., Textor, C., Wild, O., Bergmann, D. J., Bey, I., Bian, H.,
689 Cuvelier, C., Duncan, B. N., Folberth, G., Horowitz, L. W., Jonson, J., Kaminski, J. W.,
690 Marner, E., Park, R., Pringle, K. J., Schroeder, S., Szopa, S., Takemura, T., Zeng, G.,
691 Keating, T. J., and Zuber, A.: A multi-model assessment of pollution transport to the

692 Arctic, *Atmos. Chem. Phys.*, 8, 5353–5372, <https://doi.org/10.5194/acp-8-5353-2008>,
693 2008.

694 Stier, P., Feichter, J., Kinne, S., Kloster, S., Vignati, E., Wilson, J., Ganzeveld, L., Tegen, I.,
695 Werner, M., Balkanski, Y., Schulz, M., Boucher, O., Minikin, A., and Petzold, A.: The
696 aerosol-climate model ECHAM5-HAM, *Atmos. Chem. Phys.*, 5, 1125–1156,
697 doi:10.5194/acp-5-1125-2005, 2005.

698 Taylor, K. E., Williamson, D. L. and Zwiers, F. W.: The Sea Surface Temperature and Sea-
699 Ice Concentration Boundary Conditions for AMIP II Simulations, Program for Climate
700 Model Diagnosis and Intercomparison (PCMDI), Lawrence Livermore Natl. Lab.
701 Livermore, Calif., Rep., 60, 1–28 <http://www-pcmdi.llnl.gov/publications/ab60.html>,
702 2000.

703 Tegen, I., Neubauer, D., Ferrachat, S., Drian, C. S. Le, Bey, I., Schutgens, N., Stier, P.,
704 Watson-Parris, D., Stanelle, T., Schmidt, H., Rast, S., Kokkola, H., Schultz, M.,
705 Schroeder, S., Daskalakis, N., Barthel, S., Heinold, B. and Lohmann, U.: The global
706 aerosol-climate model echam6.3-ham2.3 -Part 1: Aerosol evaluation, *Geosci. Model*
707 *Dev.*, 12, 1643–1677, doi:10.5194/gmd-12-1643-2019, 2019.

708 Tegen, I., Harrison, S. P., Kohfeld, K. E., Prentice, I. C., Coe, M., and Heimann, M.: Impact
709 of vegetation and preferential source areas on global dust aerosol: Results from a model
710 study, *J. Geophys. Res.-Atmos.*, 107, 14–27, <https://doi.org/10.1029/2001JD000963>,
711 2002.

712 Waugh, D. W. and Polvani, L. M.: Intrusions into the tropical upper troposphere, *Geophys.*
713 *Res. Lett.*, 27, 3857–3860, <https://doi.org/10.1029/2000GL012250>, 2000.

714 Yan, X., Konopka, P., Hauck, M., Podglajen, A., and Ploeger, F.: Asymmetry and pathways

715 of inter-hemispheric transport in the upper troposphere and lower stratosphere, *Atmos.*
716 *Chem. Phys.*, 21, 6627–6645, <https://doi.org/10.5194/acp-21-6627-2021>, 2021.

717 Yue, J., Russell, J., Gan, Q., Wang, T., Rong, P., Garcia, R. and Mlynczak, M.: Increasing
718 Water Vapor in the Stratosphere and Mesosphere After 2002, *Geophys. Res. Lett.*, 46,
719 13452–13460, doi:10.1029/2019GL084973, 2019.

720 Zhang, K., O’Donnell, D., Kazil, J., Stier, P., Kinne, S., Lohmann, U., Ferrachat, S., Croft,
721 B., Quaas, J., Wan, H., Rast, S. and Feichter, J.: The global aerosol-climate model
722 ECHAM-HAM, version 2: Sensitivity to improvements in process representations,
723 *Atmos. Chem. Phys.*, 12, 8911–8949, doi:10.5194/acp-12-8911-2012, 2012.

724 Zheng, C., Wu, Y., Ting, M., Orbe, C., Wang, X., and Tilmes, S.: Summertime transport
725 pathways from different northern hemisphere regions into the Arctic. *Journal of*
726 *Geophysical Research: Atmospheres*, 126, e2020JD033811. [https://doi.](https://doi.org/10.1029/2020JD033811)
727 [org/10.1029/2020JD033811](https://doi.org/10.1029/2020JD033811), 2021